ACS Photonics

Open Access

pubs.acs.org/journal/apchd5

Article

Charge State Transition of Spectrally Stabilized Tin-Vacancy Centers in Diamond

Keita Ikeda, Yiyang Chen, Peng Wang, Yoshiyuki Miyamoto, Takashi Taniguchi, Shinobu Onoda, Mutsuko Hatano, and Takayuki Iwasaki*

Cite This: *ACS Photonics* 2025, 12, 2972–2981

Read Online

ACCESS | Metrics & More | Article Recommendations | Supporting Information

ABSTRACT: Solid-state quantum emitters are important platforms for quantum information processing. The fabrication of the emitters with stable photon frequency and narrow line width is a fundamental issue, and it is essential to understand optical conditions under which the emitter keeps a bright charge state or transitions to a dark state. For these purposes, in this study, we investigate the spectral stability and charge state transition of tin-vacancy (SnV) centers in diamond. The photoluminescence excitation spectra of multiple SnV centers are basically stable over time with nearly transform-limited line widths under resonant excitation, while simultaneous irradiation of resonant and nonresonant lasers makes spectra from the SnV centers unstable. We find that the instability occurs due to the charge state transition to a dark state. The charge state transition rates are quantitatively investigated depending on the laser powers. Lastly, with first-principles calculations, we model the charge state transition of the SnV center under laser irradiation.

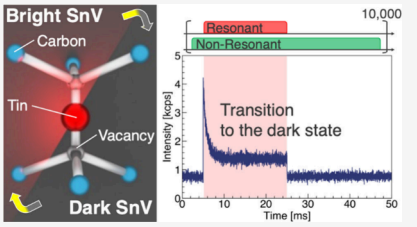

KEYWORDS: *tin-vacancy center, diamond, charge state transition, stability, quantum emitter*

INTRODUCTION

Color centers in diamond are a promising building block for quantum information processing.[1] An impurity atom and vacancy form a color center and corresponding unique energy level. The color center shows fluorescence upon laser irradiation, and its electron spin state can be also optically readout. This makes it possible to generate the spin-photon interface, which is essential for generation of remote entanglement.[2] The representative color center in diamond is a pair of a nitrogen atom and a vacancy, forming a nitrogen-vacancy (NV) center.[3] The important demonstrations for quantum network include two-photon interference,[4,5] a quantum memory over 1 min utilizing nuclear spins,[6] photon state transfer into a nuclear spin,[7,8] long-distance remote entanglement,[9,10] and entanglement among multiple qubits.[11] However, the NV center suffers from a low fraction of the zero-phonon line (ZPL) and it is subject to spectral diffusion by external noise. Alternative emerging color centers are composed of group-IV elements in the split vacancy configuration.[12,13] Among them, color centers based on the heavy atoms of tin (Sn) and lead (Pb) leads to more robustness to the effect of phonon in the ground state,[14−16] expecting a milli-second spin coherence at Kelvin temperatures, compared with the silicon-vacancy (SiV) and germanium-vacancy (GeV) centers.[17,18] Indeed, the tin-vacancy (SnV) center has been shown to have a spin coherent time of 0.3 ms for all-optical control[19] and 0.65 ms[20] and 1.57 ms[21] for microwave control at 1.7 K. A longer spin coherence time of 10 ms has been also demonstrated at 50 mK using a superconducting wire for the microwave irradiation.[22] Nuclear spins close to a SnV center can be also controlled based on dynamical decoupling techniques.[23] The SnV centers shows optical properties such as single photon emission,[14,24] transform-limited photon emission,[25,26] nearly identical photon frequencies,[27] and two-photon interference based on one SnV center.[28] Furthermore, nanophotonic and open cavity structures including SnV centers have been fabricated.[28−34]

Understanding the charge state transition of color centers in a solid-state system, including the color center itself and surrounding environment, is crucial to obtaining demanding optical and spin characteristics for quantum applications. The negatively charged state is currently known as a useful charge state of the SnV center, referred to SnV^-. A theoretical calculation suggests other charge states such as neutral state (SnV^0) and double negatively charged state (SnV^{2-}).[35] Hereinafter, the simple expression "SnV" refers to the −1 negatively charged state. Experimentally, resonant excitation to the SnV stochastically leads to the fluorescence termination, indicating the charge state conversion to a dark state.[26,36] Here, the dark state means the state which has different energy levels from the SnV center, and thus, it is not resonant to the original

Received: December 13, 2024
Revised: February 20, 2025
Accepted: February 20, 2025
Published: March 4, 2025

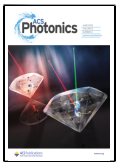

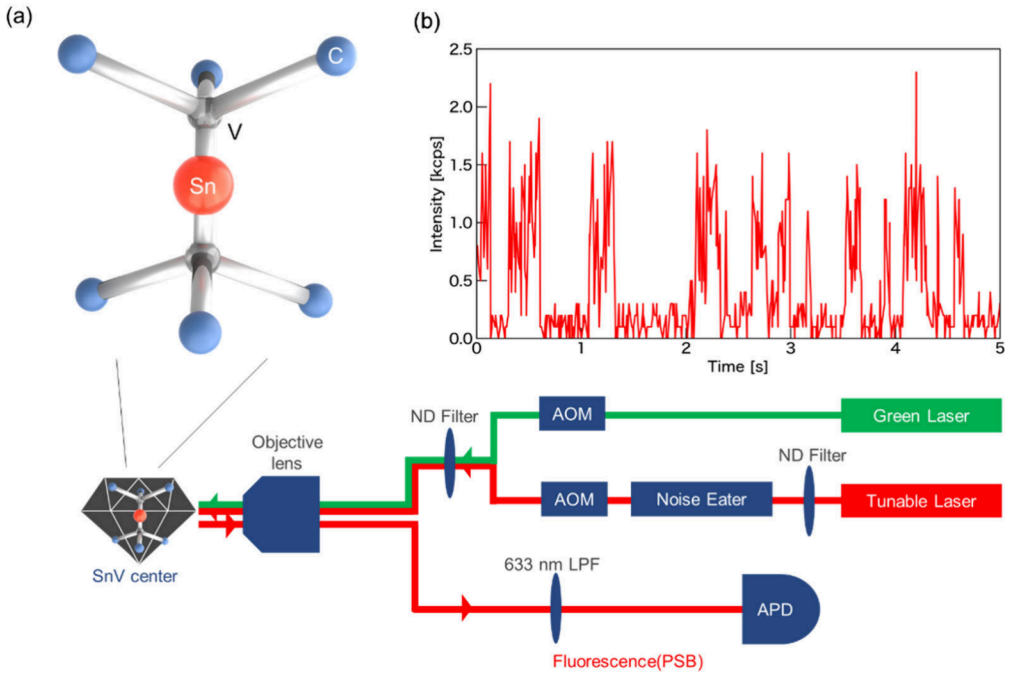

Figure 1. Experimental setup and optical response. (a) Atomic structure of a SnV center and schematic of the home-built confocal system. The blue, red, and gray spheres represent carbon, Sn, and vacancies, respectively. (b) Real-time trace under simultaneous irradiation of resonant and nonresonant lasers at 1 nW and 1 μW, respectively.

frequency of a tunable laser, i.e., around 619 nm for the SnV center. A nonresonant laser works for recovery to the bright SnV center. Thus, the nonresonant laser pulse is included at the first of the sequence for spin manipulation.[19−22] A green laser is generally used as the charge stabilization laser. However, the nonresonant laser changes the charge state of surrounding defects, resulting in spectral diffusion/jump of the color center. Recently, spectral diffusion of a SnV center was observed upon the irradiation of the nonresonant green (515 nm) laser after vanishing the fluorescence by the resonant excitation.[37] Other reports[26,36] showed that simultaneous irradiation of the resonant and nonresonant green lasers led to unstable photoluminescence excitation (PLE) spectra, probably due to spectral diffusion or charge state transition. Observation of the instability was further indicated for a pulse sequence, mentioning that the initialization of an emitter was not achieved under the simultaneous irradiation.[38] Accordingly, it is challenging to fabricate stable quantum emitters in a solid-state material and important to gain insight into the charge state dynamics when the emitter shows unstable fluorescence. In this study, we statistically observe the effect of various conditions of the laser irradiation on the stability of the high-quality SnV centers with low strain and low amount defects in the sample such that a narrow inhomogeneous distribution was obtained.[27] We find that spectral diffusion is largely suppressed for multiple SnV centers even after the nonresonant green pulse for the charge stabilization. Furthermore, we also observe unstable fluorescence upon the simultaneous irradiation of the resonant and nonresonant green lasers similar to the previous reports,[26,36] and here reveal that the dark state transition occurs using photons from both the lasers. Finally, we construct a model of the charge state transition based on first-principles calculations.

EXPERIMENTAL AND CALCULATION METHODS

The SnV centers are fabricated in IIa-type (100) single-crystal diamonds (Element Six, Electronic grade) by ion implantation followed by HPHT annealing.[27] Ion implantation is conducted at an acceleration energy of 18 MeV with a fluence of 5×10^8 cm^{-2}, resulting in a projected depth of 3 μm from the surface. Annealing treatment is performed at 2100 °C or higher under 7.7 GPa, which has been shown to generate nearly identical photon frequencies from SnV centers in previous study.[27] For all optical experiments, a home-built confocal system equipped with a cryostat is used (Figure 1a). The measurements are carried out at a low temperature of ∼6 K. A green laser (515 nm, Cobolt) is used for nonresonant excitation. Resonant excitation is performed using a dye tunable laser (Sirah Lasertechnik Matisse 2 DS). The wavelength of the dye laser is monitored by a wavemeter (Highfinesse WS8−30). Both the tunable dye laser and the 515 nm laser are intensity modulated by acousto-optic modulators (AOM, Gooch & Housego). Several fibers are used in the laser incidence system including a fiber-coupling of the two lasers[26] (not shown). The laser powers are adjusted by neutral density (ND) filters. The phonon-sideband (PSB) from the SnV center is detected through a long-pass filter (LPF) using an avalanche photo diode (APD). Confocal scanning to locate the emitters, real-time trace, and PLE measurements are performed with the Qudi python module.[39] SnV emitters and laser conditions are summarized in the Supporting Information (Table S1).

The total energy and electronic structure calculation is performed within the scheme of the density functional theory (DFT).[40,41] The cubic $3 \times 3 \times 3$ supercell corresponding to a size of 216 carbon atoms is used, and the Γ point is used for the momentum space sampling of the Bloch wave functions. The cutoff energy for the plane-wave basis is set as 64 Ry, and the norm-conserving soft pseudopotential[42] is applied to describe interactions between valence electrons and ions. The

https://doi.org/10.1021/acsphotonics.4c02490
ACS Photonics 2025, 12, 2972−2981

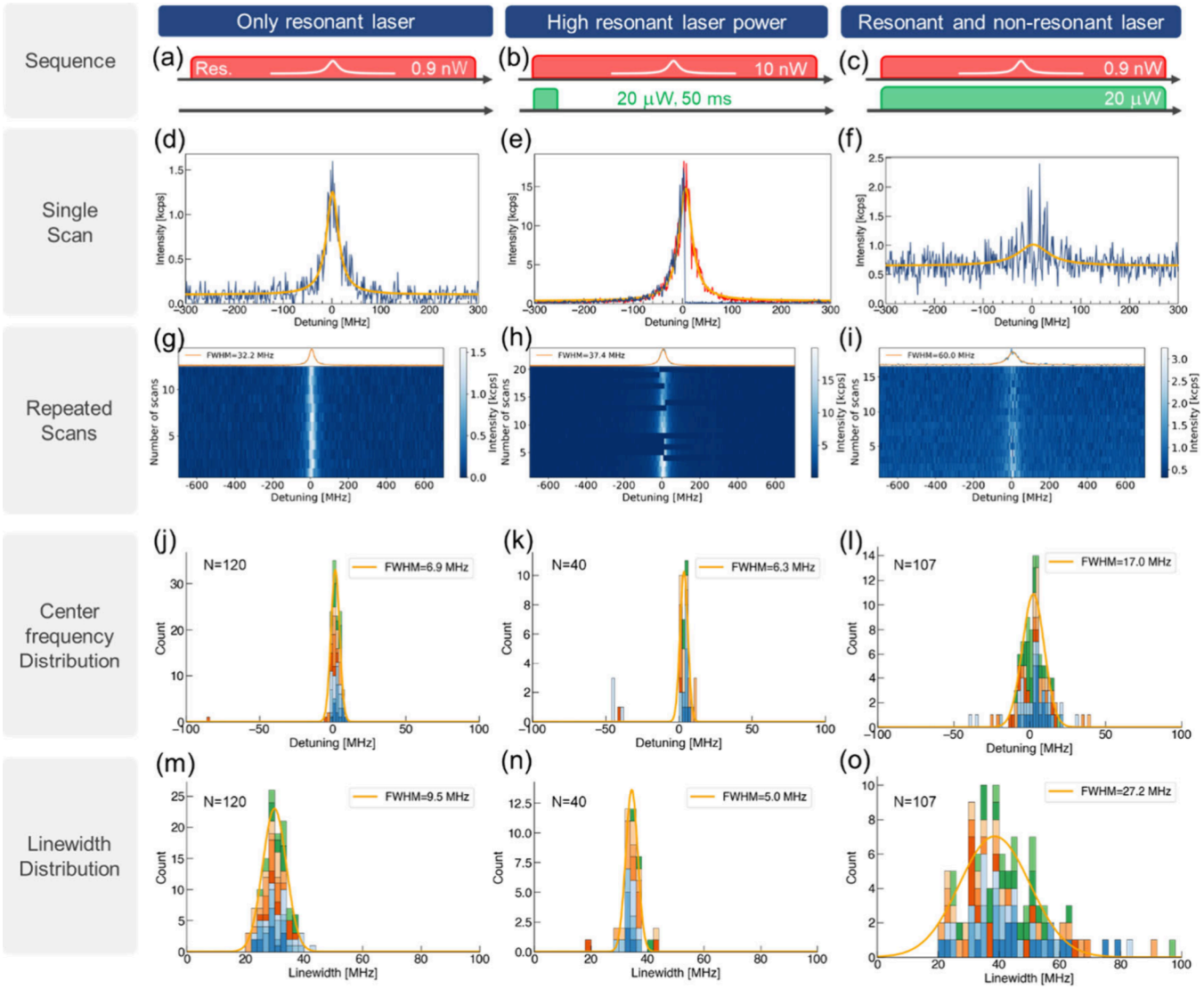

Figure 2. Consecutive PLE measurements under three optical excitation conditions. Sequence of (a) a low-power resonant laser alone, (b) a higher-power resonant laser with green charge initialization, and (c) simultaneous irradiation. (d–f) Single PLE spectra and (g–i) consecutive PLE spectra over time of one SnV center. Panel (e) shows a complete peak (red) and a scan with a sudden fluorescence termination (blue). Upper panels in g and I show averaged PLE spectra. The data with the maximum intensities in each frequency bin are used to form the peak in panel (h). Histogram of (j–l) center photon frequency and (m–o) line width of the PLE spectra of multiple emitters. Each color in the distributions corresponds to different SnV centers.

local density approximation for the exchange-correlation potential is used by employing the functional form[43] made to match the results of the uniform electron gas.[44] For the charged state, an opposite charge uniform background is taken into account to avoid the divergence of the total energy per unit cell. Atomic geometries are optimized according to the force field.[45] In order to confirm possibility of optical transitions, optical dipole matrices for individual pair of defect related orbitals

$$\int \psi_{e_u}^{*} r \psi_{e_g} \, d\boldsymbol{r}$$

are computed. Here, ψ_{e_u} and ψ_{e_g} represent calculated wave functions of the e_u and e_g states, which are labeled in Figure 6. Since the system has periodic boundary condition, the gauge conversion is taken to convert the dipole into the differential operator, so the computed matrices turn out to be

$$\int \psi_{e_u}^{*} \frac{\partial}{\partial \boldsymbol{r}} \psi_{e_g} \, d\boldsymbol{r}$$

Further examination of optical transition from states below valence top to the e_u states are performed by computing the optical matrices as

$$\int \psi_{e_u}^{*} \frac{\partial}{\partial \boldsymbol{r}} \psi_{V} \, d\boldsymbol{r}$$

Here ψ_V means wave function of states shown as dotted lines in Figure 6c.

STABILITY UNDER LASER IRRADIATION

Figure 1a shows an atomistic illustration of the SnV center in a diamond. A Sn atom is located at an interstitial position and two neighboring carbon sites become vacant. The structure has an inversion symmetry, suppressing the effect of the electrical noise from the environment. Therefore, stable fluorescence

https://doi.org/10.1021/acsphotonics.4c02490
ACS Photonics 2025, 12, 2972–2981

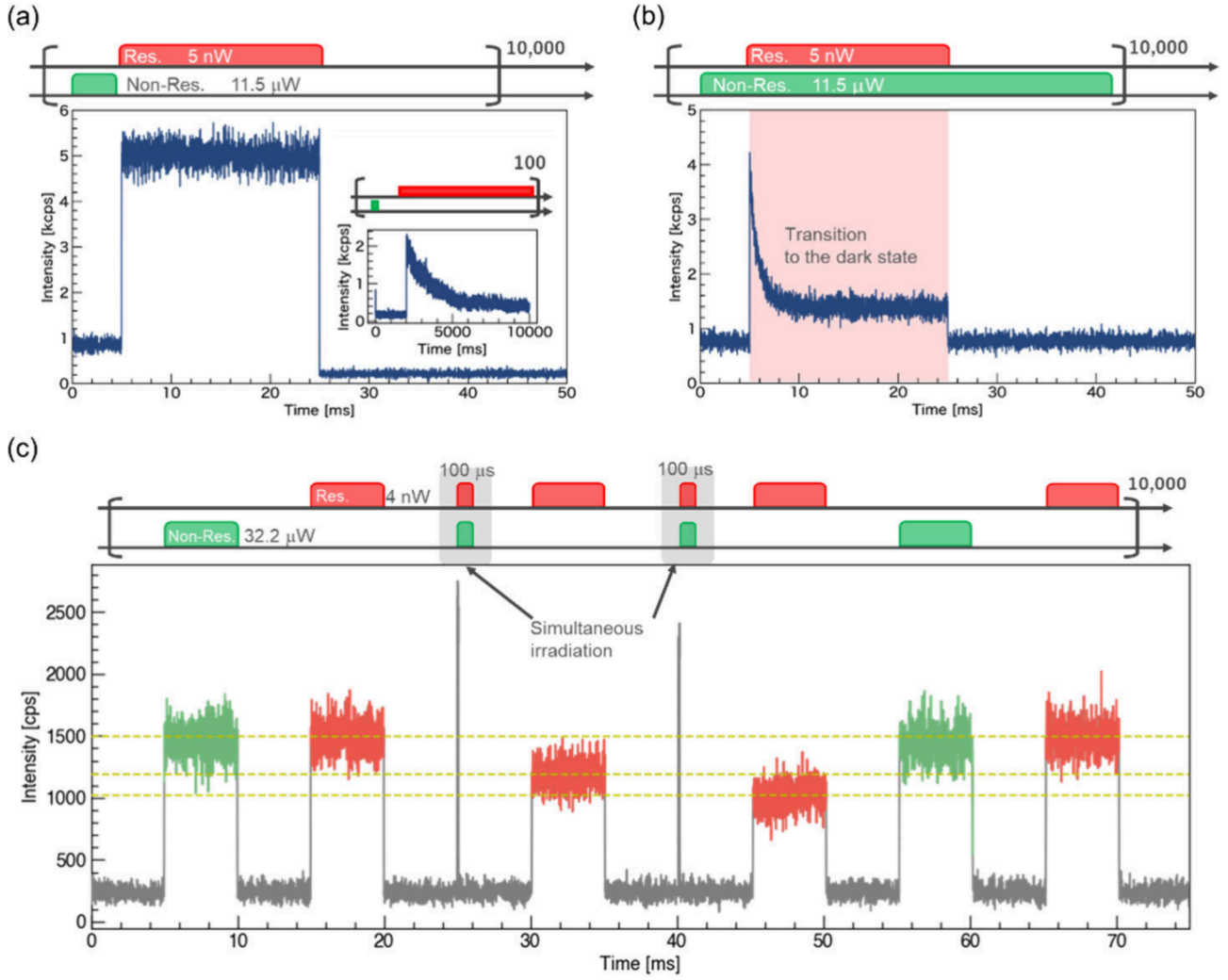

Figure 3. Pulse excitation of the SnV center. (a) Fluorescence response under resonant excitation. Repetition: 10,000 times. The inset shows a decay during a longer time scale. An 8 s resonant pulse (4 nW) is irradiated. Repetition: 100 times. (b) Fluorescence response under simultaneous irradiation of nonresonant (11.5 μW) and resonant (5 nW) lasers. Repetition: 10000 times. (c) Multipulses of simultaneous excitation. Two simultaneous excitations (0.1 ms for each) and subsequent readout resonant pulses are irradiated. In the pulse sequence in the upper panel, the pulse widths of the simultaneous irradiation are illustrated longer than the actual duration for the sake of clarity. Repetition: 10000 times. The dashed lines indicate the mean fluorescence intensities under the resonant excitation.

with less change in the photon frequency is expected for the SnV center. Four emission lines are observed from the split ground and excited states.[14] In this study, we focus on one of the four lines, called the C-peak, throughout the manuscript.

Figure 1b shows a real-time trace of the SnV fluorescence upon simultaneous irradiation of the resonant and nonresonant lasers. The count repeats the bright state with an intensity of ∼1.5 kcps and the dark state with the background level. This observation agrees with unstable PLE spectra in previous reports.[26,36] There are two possibilities for instability: a change in the photon frequency by spectral diffusion or transition of the charge state. In the following experiments, we reveal that this instability is attributed to the charge state transition of spectrally stabilized SnV centers with stable photon frequencies under resonant excitation alone.

We examine the stability of the SnV centers under three conditions of laser irradiation: weak resonant laser alone (Figure 2a), stronger resonant laser with a green pulse for initialization (Figure 2b), and simultaneous irradiation (Figure 2c). Results of the three types of measurements on one particular SnV center are shown in Figure 2d−i. We conduct these measurements for ten SnV centers for statistical analysis. For each emitter, the measurements are carried out in the order of sequence in Figure 2a, c, and b. The zero detuning in panels (g)−(l) corresponds to the center photon frequency in the first scan under only a resonant laser.

The first PLE measurements are performed with the resonant laser alone (0.9 nW), as shown in Figure 2a. The emitter shows a narrow PLE peak with a line width of 30 MHz (Figure 2d). Figure 2g shows the consecutive PLE spectra from the SnV center. The measurements are done in a Boustrophedon manner, in which once the resonant laser is scanned from right to left, then left to right, and so on. Figure 2j,m shows the summarized histograms of the center photon frequency and line width from consecutive PLE scans of the ten SnV center. The different colors correspond to the different SnV centers. The distribution of the center photon frequency has a narrow fwhm of 6.9 MHz. Note that, also including two other sequences, shifts in the center frequency by several tens of MHz are only occasionally observed (Figure

https://doi.org/10.1021/acsphotonics.4c02490
ACS Photonics 2025, 12, 2972−2981

2j–l). More details are discussed in Supporting Information (Figures S1 and S2). The histogram of the line width shows a narrow distribution with the mean value of ∼30 MHz near the transform-limited line width, estimated from an excited state lifetime of 5.2 ns.[27] This means that the SnV centers are basically stable over the measurements under irradiation by the weak resonant laser alone.

Then, we perform the second sequence including a stronger resonant laser (10 nW) for frequency scanning and a nonresonant laser pulse (515 nm, 20 μW, 50 ms) to initialize the charge state of the SnV (Figure 2b). This nonresonant laser is also likely to change the charge environment around the emitter and to induce spectral diffusion. The strong resonant excitation leads to the transition of SnV to a dark state. In addition to a complete Lorentzian peak, we also observe the termination of the fluorescence near the resonant frequency in another run (Figure 2e). The fluorescence is recovered after initialization with the green laser at the next scan in the consecutive PLE measurements (Figure 2h). The center photon frequency remains at zero detuning, and no peak appears at another position expected for spectral diffusion or jump. From more 20 times scanning for each SnV centers, we extract the data in which the fluorescence terminates in the previous scan, and then becomes a complete peak in the next scan. This analysis makes it most probable to observe spectral diffusion.[37] One emitter has no data to satisfy this condition, so we analyze the nine emitters for this sequence. We summarize the center photon frequency (Figure 2k) and line width (Figure 2n). Even with the fluorescence termination, the histogram of the center photon frequency clearly retains a narrow fwhm of 6.3 MHz similar to the resonant laser alone. This result indicates that our sample formed by the HPHT anneal has fewer defects resulting in the suppression of spectral diffusion. Note that a SnV center has multiple data at around −50 MHz detuning, but these originate from a previous different sequence (see Supporting Information, Figure S2). The slight shift of the mean line width to a higher value originates from the power broadening with the higher resonant laser power.

As the third sequence, we adopt the simultaneous irradiation of the resonant and nonresonant lasers (Figure 2c), which results in the unstable fluorescence. We find that each PLE spectrum possesses an incomplete peak, repeating the bright fluorescence and background levels, as shown in Figure 2f. This behavior agrees with the real-time trace in Figure 1b and previous reports.[26,36] Consequently, the center bright line in the consecutive PLE scans becomes apparently blurred (Figure 2i), suggesting that the SnV centers become unstable during simultaneous irradiation. We summarize the data showing a line width of 20 MHz and higher in curve fitting, comparable to those under weak resonant laser only.

Irrespective of the unstable fluorescence, the distribution of the center frequency remains around zero detuning with an fwhm of 17 MHz (Figure 2l), which is smaller than that of the line width of standard PLE spectra by only resonant laser in Figure 2m. In other words, even if a peak with a line width of 30 MHz shifts by ±8.5 MHz, the fluorescence intensity does not go down to the background level. Therefore, the spectral diffusion does not explain the observed instability under simultaneous irradiation. Although we do not exclude a possibility that small spectral diffusion occurs, broader distributions of the center photon frequency (Figure 2l) and line width (Figure 2o) would mainly come from the incomplete PLE spectra.

DARK STATE TRANSITION

Another possibility of the observed unstable fluorescence is the dark state transition of the SnV center upon the simultaneous irradiation of the resonant and nonresonant lasers. To examine the charge state transition, we investigate time variation of the fluorescence from a SnV center under resonant excitation in the absence and presence of the nonresonant laser (Figure 3a,b). We count the photon number in the phonon-sideband and repeat 10000 times for each condition. Thus, the obtained result is a histogram of the photon number with respect to the time. First, as shown in Figure 3a, we excite the emitter by resonant laser alone (5 nW) at a fixed laser frequency. The emitter does not show a fluorescence decay on the millisecond-scale, while a decay curve of the fluorescence is observed on the second-scale (inset in Figure 3a), due to the fluorescence termination induced by the change in the charge state of the emitter. We obtained a dark state transition rate of 0.6 Hz from an exponential function fit. Then, we introduce a continuous nonresonant laser (11.5 μW) together with the resonant laser pulse (5 nW), as shown in Figure 3b. During the simultaneous irradiation of the resonant and nonresonant lasers, a remarkably rapid decay of the fluorescence is observed with a rate of 1100 Hz. Following the high intensity at the start edge, the fluorescence decays and reaches a steady state. After the resonant pulse ends, the fluorescence goes down to a weaker level, coming from the diamond surface on the green laser irradiation. Since the decay is triggered by the resonant laser, it is thought to be caused by the dark state transition of the SnV center under the simultaneous irradiation, not spectral diffusion by the nonresonant green laser which is irradiated throughout the 10000 times repeated runs. Note that the nonresonant excitation also promotes the recovery to the bright state, as shown below. The two processes lead to the fluorescence intensity in the equilibrium between the fluorescence termination and recovery, in agreement with the observation of a GeV center.[46]

Next, we perform an experiment using a sequence including multipulses of the simultaneous irradiation of the resonant and nonresonant lasers, as shown in Figure 3c. After the first pulse of the nonresonant laser for the charge initialization, we apply a 5 ms resonant laser pulse to check the standard fluorescence intensity of this emitter (∼1500 cps) as a reference. Then, we apply a 0.1 ms simultaneous irradiation of the resonant and nonresonant lasers, and we again use the resonant laser alone to readout the fluorescence intensity of the emitter (∼1200 cps), which is slightly lower compared to the standard fluorescence intensity. We repeat the simultaneous irradiation-readout pulse block once more and observe a further decrease in the fluorescence intensity to ∼1000 cps. Finally, we apply a nonresonant laser pulse and subsequently readout the fluorescence intensity and find that the fluorescence intensity recovers to the standard value. The stepwise reduction in the fluorescence intensity after each pulse of the simultaneous irradiation indicates the controllability of this process, not due to stochastic spectral diffusion.

LASER POWER DEPENDENCE OF DECAY RATE

Then, we investigate the decay rate under different laser powers to examine a possible path to the dark state upon

https://doi.org/10.1021/acsphotonics.4c02490
ACS Photonics 2025, 12, 2972−2981

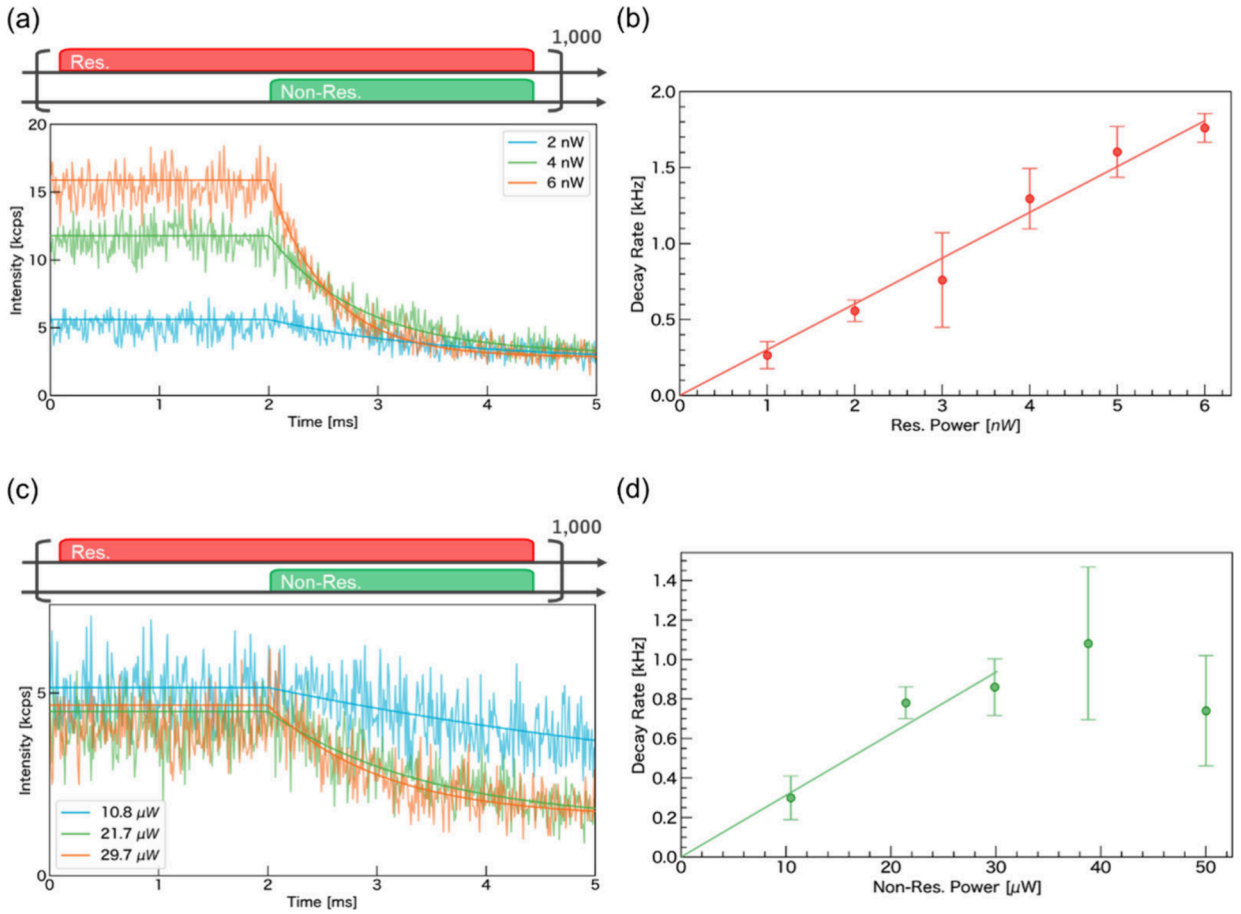

Figure 4. Decay rate. (a) Time variation and (b) decay rate as a function of the resonant laser power. (c) Time variation and (d) decay rate as a function of the nonresonant laser power. Only a portion of the total time of simultaneous irradiation is shown in panels (a) and (c). The plots in panels (b) and (d) are the average values of 5 or 3 measurements, respectively. The solid lines between 0 and 2 ms in panels (a) and (c) correspond to the values at 2 ms of each decay curve fitting. The decay rates in panels (b) and (d) are obtained from the curve fitting without considering initialization rates by the nonresonant laser because of much lower values, as seen in Figure 5. Each sequence includes an initialization pulse (omitted in the illustration of the sequences).

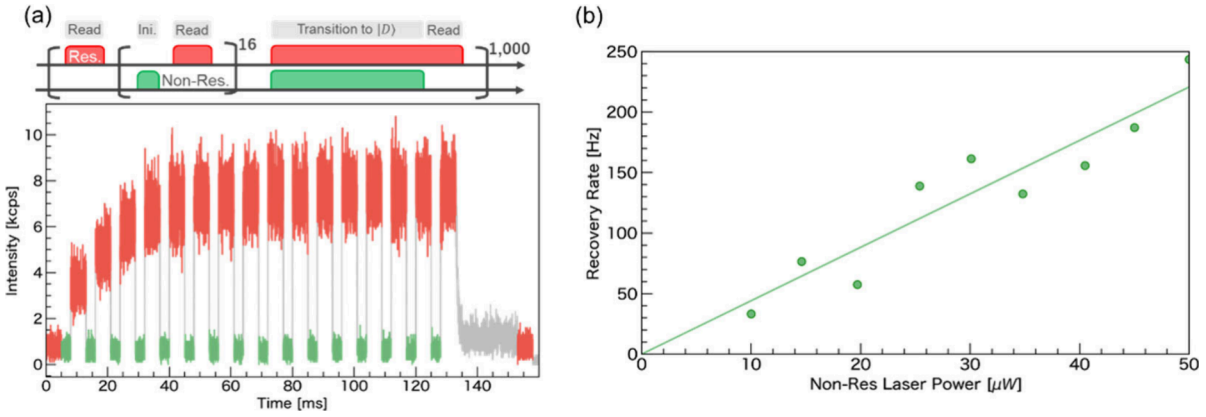

Figure 5. Recovery from the dark state. (a) Pulse sequence and observed fluorescence. (b) Recovery rate. $|D\rangle$ in the sequence denotes the dark state.

simultaneous irradiation. Figure 4a shows the decay curves at various resonant laser powers at a fixed nonresonant laser power of 20 μW. The decay becomes faster as increasing the resonant laser power, and it is well fitted linearly with a slope of 301 Hz/nW, as shown in Figure 4b. This indicates that the transition to the dark state involves one resonant photon. Importantly, here, we clearly see that the resonant laser power influences the decay rate although the emitter does not go to the dark state on this time-scale by the resonant laser alone as shown in Figure 3a. Therefore, it is thought that the resonant excitation works for efficiently making the SnV center in the excited state of the −1 charged state, and then, the SnV in the excited state goes to the dark state with addition of the nonresonant laser.

https://doi.org/10.1021/acsphotonics.4c02490
ACS Photonics 2025, 12, 2972−2981

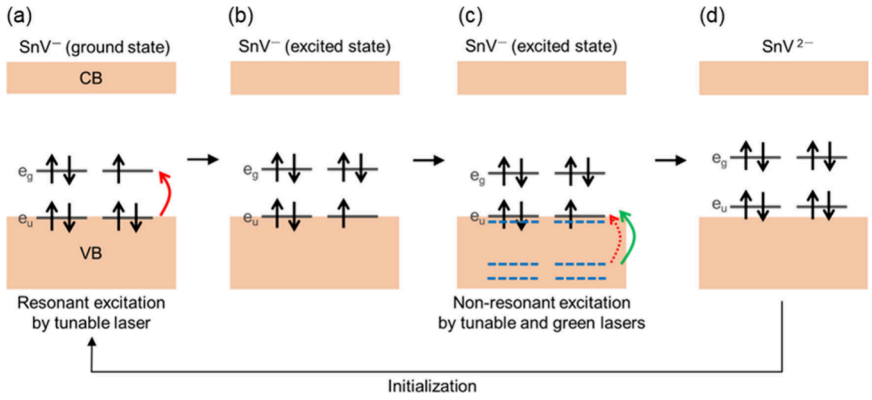

Figure 6. Model of the charge state transition. VB and CB denote the valence band and conduction band of diamond, respectively. The e_g and e_u levels are degenerate states of the SnV center. Blue dashed lines denote states in the diamond valence band, located at around 0.2, 1.6, and 2.1 eV from the e_u levels. The wavelength of the tunable laser is set to the resonance for the SnV^- excitation shown in panel (a), making it nonresonant between the e_u level and blue lines in process (c).

The dependence of the decay rate on the nonresonant laser power gives an insight into the transition process to the dark state (Figure 4c). The decay rate almost linearly increases up to 30 μW (Figure 4d). In contrast, the error bar at 40 μW becomes significantly larger and the rate drops at 50 μW. These higher powers of the nonresonant laser could cause large spectral diffusion and unstable measurements. Indeed, the simultaneous irradiation with 50 μW green laser resulted in a broad line width of 580 MHz.[26] Thus, we analyze the data up to 30 μW in Figure 4d. The linear behavior at the low power range suggests involvement of one nonresonant photon to the dark state transition. The linearity at the low powers and instability at the high powers are also observed at a different laser condition (Supporting Information, Figure S3).

RECOVERY RATE FROM DARK STATE

We observe the recovery of the fluorescence with the nonresonant green laser. Figure 5a shows the sequence and observed fluorescence from the SnV center. A 16 times-repeated block, including the nonresonant and resonant pulses, works as the gradual charge stabilization and photon counting from the SnV center, and the simultaneous irradiation is intended to change to the dark state. The fluorescence gradually increases as increasing the number of the nonresonant pulses and is saturated at around the sixth pulse. Figure 5b shows the recovery rate as a function of the nonresonant laser power. Note that, for these measurements, the initial state is not the complete dark state but the steady state upon simultaneous irradiation. As expected, basically, a higher laser power leads to a higher recovery rate to the bright state. The recovery rate has a linear dependence on the laser power, indicating that one photon in the nonresonant laser involves this recovery process.[36] The observation here mentions that the recovery occurs in a controlled manner, again evidencing the dark state transition upon simultaneous irradiation.

MODEL OF CHARGE STATE TRANSITION

Finally, we consider the mechanism of the charge state transition of the SnV center upon simultaneous irradiation. The energy levels in Figure 6 are estimated by first-principle calculations. (a) First, in the ground state of the SnV^- center, one of the e_u electrons is efficiently excited to the e_g level by absorbing one resonant photon. (b) So, the SnV^- center becomes in the excited state. (c) There are two possibilities of the dark state: SnV^0 or SnV^{2-}. Considering the underestimation of the band gap of diamond in our calculation, the energy of the 515 nm laser could not be sufficient to pump up an electron from the e_g levels in an excited SnV^- center to the conduction band of diamond. Furthermore, the calculation shows that there is no energy level near the bottom of the conduction band that accepts electrons from the e_g levels. Thus, the SnV^- does not likely go to neutral SnV^0 under this lase condition. Instead, an electron is thought to be excited from the valence band to the half-empty e_u level of the excited SnV center, with a resonant photon (red dashed arrow) or a nonresonant green photon (green solid arrow). Indeed, in the calculation, we find several energy levels in the diamond valence band from which optical excitation to the e_u level is feasible. These energy levels are denoted as the blue dashed lines. Experimentally, while the decay rate is as low as 0.6 Hz under only resonant excitation (4 nW, inset of Figure 3a), it significantly increases to ~1100 Hz under simultaneous irradiation even at a similar weak resonant laser power (5 nW). This indicates that the nonresonant green laser with a higher power of 11.5 μW included in the simultaneous irradiation contributes to this electron excitation. Thus, the dark state transition occurs quickly upon the simultaneous irradiation. Note that it is thought that the two lasers are not necessarily irradiated at the same time, but consecutive irradiation (resonant, then nonresonant excitation) with an intermediate time less than the excited state lifetime of ~5 ns[27] should work for the dark state transition. (d) When both the e_u and the e_g levels are fully occupied by electrons, the SnV center takes the −2 charge state.[36] The SnV^{2-} center has fully occupied e_u and e_g levels, and thus, there are no transition pathways, even though the optical dipole matrix has nonzero value according to our computational analysis. Then, the dark SnV^{2-} goes back to the bright SnV^- with the nonresonant laser. Our calculated results show significant energy increase of the e_g level of the SnV^{2-} state comparing SnV^- that implies the photon energy at 515 nm might pump up an electron from the e_g level in the SnV^{2-} center to the conduction band, which is consistent with a previous calculation.[35] However, we have not found particular levels in the conduction band that satisfy the optical selection rule according to the computed optical dipole matrices. Moreover, the computed levels are not as accurate as those in the previous report.[35] We here note further

https://doi.org/10.1021/acsphotonics.4c02490
ACS Photonics 2025, 12, 2972−2981

computation, which warrants precision energy levels should be applied. As another possibility, according to the model,[36] a hole is generated from an optically excited defect, e.g., a divacancy, and recombines with an electron in the SnV^{2-} center, leading to the recovery to the bright state. We need to mention that the divacancy is thought to show weak or no fluorescence due to the nonradiative decay,[47] which makes it difficult to directly evaluate the presence of the divacancies in the samples.

It is worth noting that, as another path to the dark state, there is the possibility of the direct transition from the ground state of the SnV^- center, as mentioned in a GeV center.[46] However, we exclude this possibility as the main route to the dark state for the SnV center because, as shown in Figure 4b, the dark state transition becomes faster even for the lower population in the ground state on the higher resonant laser power (a higher population in the excited state as evidenced by the increase in the fluorescence intensity in Figure 4a). Thus, it is crucial to pump up to the excited state once by the resonant laser for the dark state transition.

The dark state transition by resonant laser alone and recovery from a dark state by nonresonant laser have been reported in previous studies of SnV centers.[26,28,36] Unstable PLE spectra under the simultaneous irradiation of resonant and nonresonant lasers also agrees with previous reports.[26,36] On the other hand, in this study, we revealed that the simultaneous irradiation induces the dark state transition of the SnV center. The high-quality sample enabled us to clarify the dark-state transition, while suppressing spectral diffusion. Finally, it is worth mentioning that the efficient charge state control by the simultaneous irradiation can be applied to spin-to-charge conversion process which contributes to the high-fidelity readout of spin states.[48−50]

CONCLUSION

We investigated the spectral stability and charge state transition of the SnV centers in diamond. The resonant frequencies of the SnV centers were stable over time under resonant excitation even with the initialization pulse of the nonresonant laser. In contrast, the PLE spectra became unstable under simultaneous irradiation of the resonant and nonresonant lasers, showing the repetition of the termination and recovery of the fluorescence. We found that this phenomenon originates from the dark state transition of the SnV centers from the bright state and not spectral diffusion. The SnV center efficiently transitions to the excited state under resonant excitation, and then the transition to the dark SnV^{2-} state occurs by pumping an electron from the valence band of diamond under nonresonant laser. Although the nonresonant laser also works for initialization to the bright SnV^- state, its contribution to the dark state transition is much larger under the simultaneous irradiation. Consequently, the SnV center enters the dark state. The SnV^{2-} center goes back to the bright SnV^- center by nonresonant laser irradiation in a controlled manner. This work will contribute to achieving the fabrication of stable SnV centers and give insight into their charge state control, which are essential to construct quantum network nodes.

ASSOCIATED CONTENT

Supporting Information

The Supporting Information is available free of charge at https://pubs.acs.org/doi/10.1021/acsphotonics.4c02490.

SnV emitters and measurement conditions, instability of the SnV emission in consecutive PLE scans, and nonresonant laser power dependence on decay rate (PDF)

AUTHOR INFORMATION

Corresponding Author

Takayuki Iwasaki − *Department of Electrical and Electronic Engineering, School of Engineering, Institute of Science Tokyo, Meguro, Tokyo 152-8552, Japan;* orcid.org/0000-0001-6319-7718; Email: iwasaki.t.c5b4@m.isct.ac.jp

Authors

Keita Ikeda − *Department of Electrical and Electronic Engineering, School of Engineering, Institute of Science Tokyo, Meguro, Tokyo 152-8552, Japan*

Yiyang Chen − *Department of Electrical and Electronic Engineering, School of Engineering, Institute of Science Tokyo, Meguro, Tokyo 152-8552, Japan*

Peng Wang − *Department of Electrical and Electronic Engineering, School of Engineering, Institute of Science Tokyo, Meguro, Tokyo 152-8552, Japan;* orcid.org/0000-0002-9050-1428

Yoshiyuki Miyamoto − *Research Center for Computational Design of Advanced Functional Materials, National Institute of Advanced Industrial Science and Technology, Tsukuba, Ibaraki 305-8568, Japan;* orcid.org/0000-0001-6834-0499

Takashi Taniguchi − *Research Center for Materials Nanoarchitectonics, National Institute for Materials Science, Tsukuba 305-0044, Japan;* orcid.org/0000-0002-1467-3105

Shinobu Onoda − *Takasaki Advanced Radiation Research Institute, National Institutes for Quantum Science and Technology, Takasaki, Gunma 370-1292, Japan*

Mutsuko Hatano − *Department of Electrical and Electronic Engineering, School of Engineering, Institute of Science Tokyo, Meguro, Tokyo 152-8552, Japan*

Complete contact information is available at: https://pubs.acs.org/10.1021/acsphotonics.4c02490

Funding

This work is supported by JSPS KAKENHI Grant Number JP22H04962, the MEXT Quantum Leap Flagship Program (MEXT Q-LEAP) Grant Number JPMXS0118067395, and JST Moonshot R&D Grant Number JPMJMS2062.

Notes

The manuscript has been previously submitted to a preprint server.[51]

The authors declare no competing financial interest.

ACKNOWLEDGMENTS

We thank Y. Narita for experimental support.

REFERENCES

(1) Ruf, M.; Wan, N. H.; Choi, H.; Englund, D.; Hanson, R. Quantum Networks Based on Color Centers in Diamond. *J. Appl. Phys.* **2021**, *130*, 070901.

(2) Bernien, H.; Hensen, B.; Pfaff, W.; Koolstra, G.; Blok, M. S.; Robledo, L.; Taminiau, T. H.; Markham, M.; Twitchen, D. J.; Childress, L.; Hanson, R. Heralded Entanglement between Solid-State Qubits Separated by Three Metres. *Nature* **2013**, *497*, 86−90.

(3) Jelezko, F.; Wrachtrup, J. Single Defect Centres in Diamond: A Review. *Phys. Status Solidi Appl. Mater. Sci.* **2006**, *203*, 3207−3225.
(4) Sipahigil, A.; Goldman, M. L.; Togan, E.; Chu, Y.; Markham, M.; Twitchen, D. J.; Zibrov, A. S.; Kubanek, A.; Lukin, M. D. Quantum Interference of Single Photons from Remote Nitrogen-Vacancy Centers in Diamond. *Phys. Rev. Lett.* **2012**, *108*, 143601.
(5) Bernien, H.; Childress, L.; Robledo, L.; Markham, M.; Twitchen, D.; Hanson, R. Two-Photon Quantum Interference from Separate Nitrogen Vacancy Centers in Diamond. *Phys. Rev. Lett.* **2012**, *108*, 043604.
(6) Bradley, C. E.; Randall, J.; Abobeih, M. H.; Berrevoets, R. C.; Degen, M. J.; Bakker, M. A.; Markham, M.; Twitchen, D. J.; Taminiau, T. H. A Ten-Qubit Solid-State Spin Register with Quantum Memory up to One Minute. *Phys. Rev. X* **2019**, *9*, 31045.
(7) Yang, S.; Wang, Y.; Rao, D. D. B.; Hien Tran, T.; Momenzadeh, A. S.; Markham, M.; Twitchen, D. J.; Wang, P.; Yang, W.; Stohr, R.; Neumann, P.; Kosaka, H.; Wrachtrup, J. High-Fidelity Transfer and Storage of Photon States in a Single Nuclear Spin. *Nat. Photonics* **2016**, *10*, 507−511.
(8) Tsurumoto, K.; Kuroiwa, R.; Kano, H.; Sekiguchi, Y.; Kosaka, H. Quantum Teleportation-Based State Transfer of Photon Polarization into a Carbon Spin in Diamond. *Commun. Phys.* **2019**, *2*, 74.
(9) Hensen, B.; Bernien, H.; Dreaú, A. E.; Reiserer, A.; Kalb, N.; Blok, M. S.; Ruitenberg, J.; Vermeulen, R. F. L.; Schouten, R. N.; Abellán, C.; Amaya, W.; Pruneri, V.; Mitchell, M. W.; Markham, M.; Twitchen, D. J.; Elkouss, D.; Wehner, S.; Taminiau, T. H.; Hanson, R. Loophole-Free Bell Inequality Violation Using Electron Spins Separated by 1.3 Kilometres. *Nature* **2015**, *526*, 682−686.
(10) Stolk, A. J.; van der Enden, K. L.; Slater, M.-C.; te Raa-Derckx, I.; Botma, P.; van Rantwijk, J.; Biemond, J. J. B.; Hagen, R. A. J.; Herfst, R. W.; Koek, W. D.; Meskers, A. J. H.; Vollmer, R.; van Zwet, E. J.; Markham, M.; Edmonds, A. M.; Geus, J. F.; Elsen, F.; Jungbluth, B.; Haefner, C.; Tresp, C.; Stuhler, J.; Ritter, S.; Hanson, R. Metropolitan-Scale Heralded Entanglement of Solid-State Qubits. *Sci. Adv.* **2024**, *10*, No. eadp6442.
(11) Pompili, M.; Hermans, S. L. N.; Baier, S.; Beukers, H. K. C.; Humphreys, P. C.; Schouten, R. N.; Vermeulen, R. F. L.; Tiggelman, M. J.; dos Santos Martins, L.; Dirkse, B.; Wehner, S.; Hanson, R. Realization of a Multinode Quantum Network of Remote Solid-State Qubits. *Science* **2021**, *372*, 259−264.
(12) Iwasaki, T. Color Centers Based on Heavy Group-IV Elements. *Semicond. Semimetals* **2020**, *103*, 237−256.
(13) Bradac, C.; Gao, W.; Forneris, J.; Trusheim, M. E.; Aharonovich, I. Quantum Nanophotonics with Group IV Defects in Diamond. *Nat. Commun.* **2019**, *10*, 5625.
(14) Iwasaki, T.; Miyamoto, Y.; Taniguchi, T.; Siyushev, P.; Metsch, M. H.; Jelezko, F.; Hatano, M. Tin-Vacancy Quantum Emitters in Diamond. *Phys. Rev. Lett.* **2017**, *119*, 253601.
(15) Wang, P.; Taniguchi, T.; Miyamoto, Y.; Hatano, M.; Iwasaki, T. Low-Temperature Spectroscopic Investigation of Lead-Vacancy Centers in Diamond Fabricated by High-Pressure and High-Temperature Treatment. *ACS Photonics* **2021**, *8*, 2947−2954.
(16) Wang, P.; Kazak, L.; Senkalla, K.; Siyushev, P.; Abe, R.; Taniguchi, T.; Onoda, S.; Kato, H.; Makino, T.; Hatano, M.; Jelezko, F.; Iwasaki, T. Transform-Limited Photon Emission from a Lead-Vacancy Center in Diamond above 10 K. *Phys. Rev. Lett.* **2024**, *132*, 073601.
(17) Sukachev, D. D.; Sipahigil, A.; Nguyen, C. T.; Bhaskar, M. K.; Evans, R. E.; Jelezko, F.; Lukin, M. D. Silicon-Vacancy Spin Qubit in Diamond: A Quantum Memory Exceeding 10 ms with Single-Shot State Readout. *Phys. Rev. Lett.* **2017**, *119*, 223602.
(18) Senkalla, K.; Genov, G.; Metsch, M. H.; Siyushev, P.; Jelezko, F. Germanium Vacancy in Diamond Quantum Memory Exceeding 20 ms. *Phys. Rev. Lett.* **2024**, *132*, 26901.
(19) Debroux, R.; Michaels, C. P.; Purser, C. M.; Wan, N.; Trusheim, M. E.; Arjona Martínez, J.; Parker, R. A.; Stramma, A. M.; Chen, K. C.; de Santis, L.; Alexeev, E. M.; Ferrari, A. C.; Englund, D.; Gangloff, D. A.; Atatüre, M. Quantum Control of the Tin-Vacancy Spin Qubit in Diamond. *Phys. Rev. X* **2021**, *11*, 041041.
(20) Rosenthal, E. I.; Anderson, C. P.; Kleidermacher, H. C.; Stein, A. J.; Lee, H.; Grzesik, J.; Scuri, G.; Rugar, A. E.; Riedel, D.; Aghaeimeibodi, S.; Ahn, G. H.; Van Gasse, K.; Vučković, J. Microwave Spin Control of a Tin-Vacancy Qubit in Diamond. *Phys. Rev. X* **2023**, *13*, 031022.
(21) Guo, X.; Stramma, A. M.; Li, Z.; Roth, W. G.; Huang, B.; Jin, Y.; Parker, R. A.; Arjona Martínez, J.; Shofer, N.; Michaels, C. P.; Purser, C. P.; Appel, M. H.; Alexeev, E. M.; Liu, T.; Ferrari, A. C.; Awschalom, D. D.; Delegan, N.; Pingault, B.; Galli, G.; Heremans, F. J.; Atatüre, M.; High, A. A. Microwave-Based Quantum Control and Coherence Protection of Tin-Vacancy Spin Qubits in a Strain-Tuned Diamond-Membrane Heterostructure. *Phys. Rev. X* **2023**, *13*, 041037.
(22) Karapatzakis, I.; Resch, J.; Schrodin, M.; Fuchs, P.; Kieschnick, M.; Heupel, J.; Kussi, L.; Sürgers, C.; Popov, C.; Meijer, J.; Becher, C.; Wernsdorfer, W.; Hunger, D. Microwave Control of the Tin-Vacancy Spin Qubit in Diamond with a Superconducting Waveguide. *Phys. Rev. X* **2024**, *14*, 31036.
(23) Beukers, H. K. C.; Waas, C.; Pasini, M.; Ommen, H. B. Van; Codreanu, N.; Julia, M.; Turan, T.; Iuliano, M.; Ademi, Z.; Taminiau, T. H.; Hanson, R. Control of Solid-State Nuclear Spin Qubits Using an Electron Spin-1/2. 2024. 2409.08977. arXiv. https//arxiv.org/abs/2409.08977 (accessed Sep. 17, 2024).
(24) Tchernij, S. D.; Herzig, T.; Forneris, J.; Küpper, J.; Pezzagna, S.; Traina, P.; Moreva, E.; Degiovanni, I. P.; Brida, G.; Skukan, N.; Genovese, M.; Jakšić, M.; Meijer, J.; Olivero, P. Single-Photon-Emitting Optical Centers in Diamond Fabricated upon Sn Implantation. *ACS Photonics* **2017**, *4*, 2580−2586.
(25) Trusheim, M. E.; Pingault, B.; Wan, N. H.; Gündoğan, M.; De Santis, L.; Debroux, R.; Gangloff, D.; Purser, C.; Chen, K. C.; Walsh, M.; Rose, J. J.; Becker, J. N.; Lienhard, B.; Bersin, E.; Paradeisanos, I.; Wang, G.; Lyzwa, D.; Montblanch, A. R. P.; Malladi, G.; Bakhru, H.; Ferrari, A. C.; Walmsley, I. A.; Atatüre, M.; Englund, D. Transform-Limited Photons from a Coherent Tin-Vacancy Spin in Diamond. *Phys. Rev. Lett.* **2020**, *124*, 023602.
(26) Gorlitz, J.; Herrmann, D.; Thiering, G.; Fuchs, P.; Gandil, M.; Iwasaki, T.; Taniguchi, T.; Kieschnick, M.; Meijer, J.; Hatano, M.; Gali, A.; Becher, C. Spectroscopic Investigations of Negatively Charged Tin-Vacancy Centres in Diamond. *New J. Phys.* **2020**, *22*, 013048.
(27) Narita, Y.; Wang, P.; Ikeda, K.; Oba, K.; Miyamoto, Y.; Taniguchi, T.; Onoda, S.; Hatano, M.; Iwasaki, T. Multiple Tin-Vacancy Centers in Diamond with Nearly Identical Photon Frequency and Linewidth. *Phys. Rev. Appl.* **2023**, *19*, 024061.
(28) Arjona Martinez, J.; Parker, R. A.; Chen, K. C.; Purser, C. M.; Li, L.; Michaels, C. P.; Stramma, A. M.; Debroux, R.; Harris, I. B.; Hayhurst Appel, M.; Nichols, E. C.; Trusheim, M. E.; Gangloff, D. A.; Englund, D.; Atature, M. Photonic Indistinguishability of the Tin-Vacancy Center in Diamond. *Phys. Rev. Lett.* **2022**, *129*, 173603.
(29) Parker, R. A.; Arjona Martínez, J.; Chen, K. C.; Stramma, A. M.; Harris, I. B.; Michaels, C. P.; Trusheim, M. E.; Hayhurst Appel, M.; Purser, C. M.; Roth, W. G.; Englund, D.; Atatüre, M. A Diamond Nanophotonic Interface with an Optically Accessible Deterministic Electronuclear Spin Register. *Nat. Photonics* **2024**, *18*, 156−161.
(30) Rugar, A. E.; Aghaeimeibodi, S.; Riedel, D.; Dory, C.; Lu, H.; McQuade, P. J.; Shen, Z. X.; Melosh, N. A.; Vučković, J. Quantum Photonic Interface for Tin-Vacancy Centers in Diamond. *Phys. Rev. X* **2021**, *11*, 031021.
(31) Pasini, M.; Codreanu, N.; Turan, T.; Riera Moral, A.; Primavera, C. F.; De Santis, L.; Beukers, H. K. C.; Brevoord, J. M.; Waas, C.; Borregaard, J.; Hanson, R. Nonlinear Quantum Photonics with a Tin-Vacancy Center Coupled to a One-Dimensional Diamond Waveguide. *Phys. Rev. Lett.* **2024**, *133*, 023603.
(32) Herrmann, Y.; Fischer, J.; Brevoord, J. M.; Sauerzapf, C.; Wienhoven, L. G. C.; Feije, L. J.; Pasini, M.; Eschen, M.; Ruf, M.; Weaver, M. J.; Hanson, R. Coherent Coupling of a Diamond Tin-Vacancy Center to a Tunable Open Microcavity. *Phys. Rev. X* **2024**, *14*, 041013.
(33) Kuruma, K.; Pingault, B.; Chia, C.; Renaud, D.; Hoffmann, P.; Iwamoto, S.; Ronning, C.; Lončar, M. Coupling of a Single Tin-

Vacancy Center to a Photonic Crystal Cavity in Diamond. *Appl. Phys. Lett.* **2021**, *118*, 230601.
(34) Li, L.; Santis, L. De; Harris, I. B. W.; Chen, K. C.; Gao, Y.; Christen, I.; Choi, H.; Trusheim, M.; Song, Y.; Errando-Herranz, C.; Du, J.; Hu, Y.; Clark, G.; Ibrahim, M. I.; Gilbert, G.; Han, R.; Englund, D. Heterogeneous Integration of Spin-Photon Interfaces with a CMOS Platform. *Nature* **2024**, *630*, 70−76.
(35) Thiering, G.; Gali, A. Ab Initio Magneto-Optical Spectrum of Group-IV Vacancy Color Centers in Diamond. *Phys. Rev. X* **2018**, *8*, 021063.
(36) Görlitz, J.; Herrmann, D.; Fuchs, P.; Iwasaki, T.; Taniguchi, T.; Rogalla, D.; Hardeman, D.; Colard, P. O.; Markham, M.; Hatano, M.; Becher, C. Coherence of a Charge Stabilised Tin-Vacancy Spin in Diamond. *npj Quantum Inf.* **2022**, *8*, 45.
(37) Brevoord, J. M.; De Santis, L.; Yamamoto, T.; Pasini, M.; Codreanu, N.; Turan, T.; Beukers, H. K. C.; Waas, C.; Hanson, R. Heralded Initialization of Charge State and Optical-Transition Frequency of Diamond Tin-Vacancy Centers. *Phys. Rev. Appl.* **2024**, *21*, 054047.
(38) Debroux, R. Developing the Spin Qubit of the Tin-Vacancy Center in Diamond for Quantum Networks. Ph.D Diss. Univ. Cambridge, Cambridge, 2022.
(39) Binder, J. M.; Stark, A.; Tomek, N.; Scheuer, J.; Frank, F.; Jahnke, K. D.; Müller, C.; Schmitt, S.; Metsch, M. H.; Unden, T.; Gehring, T.; Huck, A.; Andersen, U. L.; Rogers, L. J.; Jelezko, F. Qudi: A Modular Python Suite for Experiment Control and Data Processing. *SoftwareX* **2017**, *6*, 85−90.
(40) Hohenberg, P.; Kohn, W. Inhomogeneous Electron Gas. *Phys. Rev.* **1964**, *136*, B864−B871.
(41) Kohn, W.; Sham, L. J. Self-Consistent Equations Including Exchange and Correlation Effects. *Phys. Rev.* **1965**, *140*, A1133−1138.
(42) Troullier, N.; Martins, J. L. Efficient Pseudopotentials for Plane-Wave Calculations. *Phys. Rev. B* **1991**, *43*, 1993−2006.
(43) Perdew, J. P.; Zunger, A. Self-Interaction Correction to Density-Functional Approximations for Many-Electron Systems. *Phys. Rev. B* **1981**, *23*, 5048−5079.
(44) Ceperley, D. M.; Alder, B. J. Ground State of the Electron Gas by a Stochastic Method. *Phys. Rev. Lett.* **1980**, *45*, 566−569.
(45) Ihm, J.; Zunger, A.; Cohen, M. L. Momentum-Space Formalism for the Total Energy of Solids. *J. Phys. C Solid State Phys.* **1979**, *12*, 4409−4422.
(46) Chen, D.; Mu, Z.; Zhou, Y.; Fröch, J. E.; Rasmit, A.; Diederichs, C.; Zheludev, N.; Aharonovich, I.; Gao, W. B. Optical Gating of Resonance Fluorescence from a Single Germanium Vacancy Color Center in Diamond. *Phys. Rev. Lett.* **2019**, *123*, 033602.
(47) Miyamoto, Y. Decay Process of Photoexcited Divacancies in Diamond Studied by First-Principles Simulations. *Phys. Rev. Mater.* **2023**, *7*, 086002.
(48) Zhang, Q.; Guo, Y.; Ji, W.; Wang, M.; Yin, J.; Kong, F.; Lin, Y.; Yin, C.; Shi, F.; Wang, Y.; Du, J. High-Fidelity Single-Shot Readout of Single Electron Spin in Diamond with Spin-to-Charge Conversion. *Nat. Commun.* **2021**, *12*, 1529.
(49) Rosenthal, E. I.; Biswas, S.; Scuri, G.; Lee, H.; Stein, A. J.; Kleidermacher, H. C.; Grzesik, J.; Rugar, A. E.; Aghaeimeibodi, S.; Riedel, D.; Titze, M.; Bielejec, E. S.; Choi, J.; Anderson, C. P.; Vuckovic, J. Single-Shot Readout and Weak Measurement of a Tin-Vacancy Qubit in Diamond. *Phys. Rev. X***2024**, *14*, 041008.
(50) Shields, B. J.; Unterreithmeier, Q. P.; De Leon, N. P.; Park, H.; Lukin, M. D. Efficient Readout of a Single Spin State in Diamond via Spin-to-Charge Conversion. *Phys. Rev. Lett.* **2015**, *114*, 136402.
(51) Ikeda, K.; Chen, Y.; Wang, P.; Miyamoto, Y.; Taniguchi, T.; Onoda, S.; Hatano, M.; Iwasaki, T. Charge State Transition of Spectrally Stabilized Tin-Vacancy Centers in Diamond. 2024. 2412.07087. arXiv. https//arxiv.org/abs/2412.07087 (accessed Dec. 11, 2024).

https://doi.org/10.1021/acsphotonics.4c02490
ACS Photonics 2025, 12, 2972−2981